

Planning for quasi-static manipulation tasks via an intrinsic haptic metric

Lin Yang, Sri Harsha Turlapati, Chen Lv, Domenico Campolo*

Abstract—Contact-rich manipulation often requires strategic interactions with objects, such as pushing to accomplish specific tasks. We propose a novel scenario where a robot inserts a book into a crowded shelf by pushing aside neighboring books to create space before slotting the new book into place. Classical planning algorithms fail in this context due to limited space and their tendency to avoid contact. Additionally, they do not handle indirectly manipulable objects or consider force interactions. Our key contributions are: *i*) re-framing quasi-static manipulation as a planning problem on an implicit manifold derived from equilibrium conditions; *ii*) utilizing an intrinsic haptic metric instead of ad-hoc cost functions; and *iii*) proposing an adaptive algorithm that simultaneously updates robot states, object positions, contact points, and haptic distances. We evaluate our method on such crowded bookshelf insertion task but it is a general formulation to rigid bodies manipulation tasks. We propose proxies to capture contact point and force, with superellipse to represent objects. This simplified model guarantee the differentiability. Our framework autonomously discovers strategic wedging-in policies while our simplified contact model achieves behavior similar to real world scenarios. We also vary the stiffness and initial positions to analysis our framework comprehensively. The video can be found at <https://youtu.be/eab8umZ3AQ0>.

Index Terms—Manipulation planning, manifold constraints, haptic metric, haptic obstacle, quasi-static manipulation, crowded bookshelf insertion.

I. INTRODUCTION

Robotic manipulation is a challenging area that not only requires conventional motion planning but also the ability to make and maintain physical contact with objects [1]. Traditional motion planning primarily focuses on avoiding collisions, making it suitable for navigating free spaces. However, when it comes to contact-rich tasks, such as inserting a book into a crowded shelf, traditional methods often fail, as these scenarios require strategic use of force and contact. For example, as illustrated in Fig. 1a, traditional motion planning would struggle due to limited space for maneuvering the book. This highlights a broader challenge in robotics: how to handle tasks that require strategic policy and controlled contact interactions.

There have been numerous efforts to integrate contact constraints within the configuration space (C-space) of motion planning, where these constraints generate manifold. Some planners enable robots to navigate on the constraint manifold [2]. Techniques like relaxation [3], projection [4], tangent

All authors are with the School of Mechanical and Aerospace Engineering, Nanyang Technological University (NTU), Singapore.

* Corresponding author: d.campolo@ntu.edu.sg

This research is supported by the National Research Foundation, Singapore, under the NRF Medium Sized Centre scheme (CARTIN).

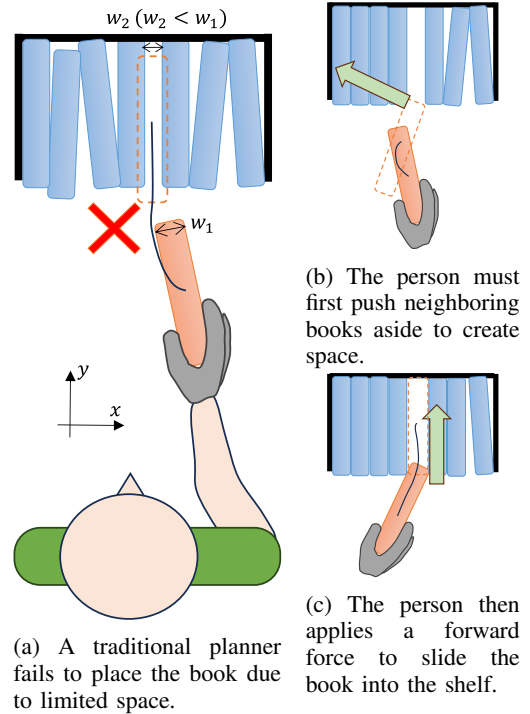


Fig. 1: Inserting a book into a crowded shelf filled with other books (blue), where the space is insufficient for a new book (orange).

space [5], AtlasRRT [6], and implicit manifold configuration space (IMACS) [7] have been explored to handle these constraints. However, these methods mainly address geometric constraints, lacking the capability to manage force interactions, which are critical in tasks like the aforementioned book insertion. While some advanced formulations consider both robot and object configurations, they often fail to explicitly model force interactions [8] or lack an intrinsic metric to evaluate such spaces [9].

In contrast to the planning algorithms mentioned above, reinforcement learning (RL) has also been applied to contact-rich manipulation tasks using physical simulators [10]. While some model-free algorithms are capable of handling these tasks after extensive exploration, they often require detailed environment models and use task-specific cost functions [11]. In our approach, we replace these ad-hoc cost functions with an intrinsic haptic metric, which offers a more general measure of interaction. Furthermore, RL models face challenges when incorporating force information due to the sim2real gap. Col-

lecting real world haptic data can mitigate this issue, but it is a time-consuming process (e.g., over 10 hours [12]). To address these challenges, we leverage a combination of dynamic movement primitives (DMP) and black-box optimization (BBO) [13]. This approach simplifies the learning problem, allowing for efficient exploration in a low-dimensional parameter space while minimising the haptic distance computed by intrinsic haptic metric, which intuitively optimises the force during manipulation.

Significant research has focused on predicting contact forces in interaction tasks, such as Peg-in-Hole assembly [14]. Traditional approaches rely on (i) predefined compliant structures, (ii) precise geometry information, and (iii) user-defined contact phases [15], [16]. The compliant supports are crucial to avoid jamming, which can cause failure in tight-insertion scenarios. Within this scope, in this work, we propose a novel quasi-static manipulation [17], [18] framework endowed with an *intrinsic* haptic metric. This enables in contrast to the above-defined three-step approach (a) impedance controlled manipulation, (b) handling arbitrary object geometries, and (c) automatic evolution of contact phases based on equilibrium states, without the need for extensive pre-definition. We highlight that our novelty lies in the intrinsic nature of our framework in defining manipulation potentials that capture both physical interaction and robot impedance control.

Our framework requires only a manipulation potential to describe the entire system. This potential energy includes (i) robot impedance control [19], where control springs store potential energy, and (ii) physical contact modeled by energy model (e.g., [20]). The manipulation potential with quasi-static assumption defines a differentiable manifold, which is crucial for optimization. Differentiable simulation, as noted by [21], offers advantages in task inversion, thus facilitates further optimization. To ensure model differentiability, we utilize superellipse-based object representations, and proxies capturing contact point, to guarantee the differentiability.

Our work builds on a recent framework for quasi-static manipulation [17], [18], which relies on a single *potential* function to formally describe the manipulation system. This approach reformulates the robot-environment interaction as a control problem by splitting variables into internal states \mathbf{z} and control inputs \mathbf{u} . The inputs \mathbf{u} guide the movement of uncontrollable states \mathbf{z} along an implicitly defined equilibrium manifold (\mathcal{M}^{eq}). We extend this framework by introducing a haptic planning algorithm within this partitioned space, relying solely on a manipulation potential to characterize the environment. Our method utilizes an adaptive algorithm that continuously updates: (i) the haptic distance using an intrinsic haptic metric, and (ii) the positions of the robot, uncontrollable objects, and contact points. This framework is validated through a challenging crowded book insertion task, where our approach autonomously discovers optimal wedging-in strategies. Additionally, our experiments and simulations show a consistent trend in contact forces. Furthermore, by adjusting task stiffness, the method adapts to interact with low-stiffness neighboring objects, demonstrating flexibility in

varying environments.

II. MOTION PLANNING ON EQUILIBRIUM MANIFOLD

In this section, we detail our configuration space and the key components, e.g., haptic metric, haptic distance and adaptive Ordinary Differential Equations (ODE).

A. Quasi-Static Mechanical Manipulation System

Under the assumption of quasi-static motions, the mechanical robot-environment interaction is reformulated as a control problem via splitting of variables $\mathcal{Z} \times \mathcal{U}$ [17], [18], where $\mathbf{z} \in \mathcal{Z} \subset \mathbb{R}^N$ is the *internal state* (also referred to as uncontrollable objects) and $\mathbf{u} \in \mathcal{U} \subset \mathbb{R}^K$ is the *control* of the robot (which can be interpreted as the desired pose in impedance control). The configuration of the system is determined solely by its potential energies, such as elastic and gravitational energies, which we refer to as the manipulation potential $W(\mathbf{z}, \mathbf{u})$. Define manipulation potential as a smooth field on the space $W : \mathcal{Z} \times \mathcal{U} \rightarrow \mathbb{R}$. For any given control \mathbf{u} , equilibria of system satisfy

$$\partial_{\mathbf{z}} W(\mathbf{z}^*(\mathbf{u}), \mathbf{u}) = \mathbf{0} \in \mathbb{R}^N. \quad (1)$$

We define $\partial_{\mathbf{q}} W \equiv [\partial_{q_1} W, \dots, \partial_{q_a} W]^T$, where the *partial* (column) operator is defined as $\partial_{\mathbf{q}} = [\partial_{q_1}, \dots, \partial_{q_a}]^T$. Meanwhile, define the shorthand notation $\partial_{\mathbf{z}}^2 \equiv (\partial_{\mathbf{z}} \partial_{\mathbf{z}}^T) = \partial_{\mathbf{z}} \partial_{\mathbf{z}}^T$ for Hessians and mixed-derivative operators. Hence, in Eq. 1, $\partial_{\mathbf{z}}$ denotes the gradient with respect to \mathbf{z} , which means internal forces acting on objects \mathbf{z} . Under the quasi-static assumption, the total force acting on the objects should be zero.

A point is strictly stable when its Hessian is positive definite, i.e., $\partial_{\mathbf{z}\mathbf{z}}^2 W|_* \succ 0$. Assuming the Hessian $\partial_{\mathbf{z}\mathbf{z}}^2 W \in \mathbb{R}^{N \times N}$ is of full rank when $\partial_{\mathbf{z}} W(\mathbf{z}^*, \mathbf{u}) = \mathbf{0}$, via the *implicit function theorem* [22], the set

$$\mathcal{M}^{eq} := \{(\mathbf{z}, \mathbf{u}) \in \mathcal{Z} \times \mathcal{U} | \partial_{\mathbf{z}} W(\mathbf{z}, \mathbf{u}) = \mathbf{0}\} \quad (2)$$

is a smooth embedded submanifold in the ambient space ($\mathcal{Z} \times \mathcal{U}$). We refer to \mathcal{M}^{eq} as the *equilibrium manifold* of the system. Under the quasi-static assumption, the external force equals the control force. Thus, from the robot's perspective, it can use its joint torque sensors to estimate the external contact force. We define the control forces as $\mathbf{f}_{ctrl} = -\partial_{\mathbf{u}} W$ is called *control forces* [17].

B. Haptic Metric and Haptic Distance

The closeness of states is determined by a distance function. In the context of quasi-static manipulations, we choose the *haptic metric* as the Riemannian metric of the control space \mathcal{U} . Following [17] the *control Hessian* of an interconnected system with a potential $W : \mathcal{Z} \times \mathcal{U} \rightarrow \mathbb{R}$ is defined as:

$$\mathbf{G}_m(\mathbf{z}^*(\mathbf{u}), \mathbf{u}) := \partial_{\mathbf{u}\mathbf{u}}^2 W - \partial_{\mathbf{u}\mathbf{z}}^2 W (\partial_{\mathbf{z}\mathbf{z}}^2 W)^{-1} \partial_{\mathbf{z}\mathbf{u}}^2 W, \quad (3)$$

This is computed as the Schur's complement of the Hessian of the potential $W(\mathbf{z}_m^*, \mathbf{u})$, evaluated at equilibrium (i.e., $\mathbf{z}^*(\mathbf{u})$ s.t. $\partial_{\mathbf{z}} W(\mathbf{z}^*, \mathbf{u}) = \mathbf{0}$), and $\partial_{\mathbf{u}\mathbf{z}}^2 W = (\partial_{\mathbf{z}\mathbf{u}}^2 W)^T \in \mathbb{R}^{K \times N}$. The squared Hessian $\mathbf{G}_m^2(\mathbf{z}^*(\mathbf{u}), \mathbf{u})$ is called the *haptic metric*¹, which is at least positive semi-definite.

To understand the concept of a haptic metric, consider the example of an inverted pendulum in [17]. \mathcal{M}^{eq} for manipulating the inverted pendulum takes the form of a staircase, represented by the orange dots in Fig. 2. The haptic metric is illustrated as a blue ellipse, defined by the equation $\mathbf{u}^T \mathbf{G}_m^2(\mathbf{z}^*(\mathbf{u}), \mathbf{u}) \mathbf{u} = 1$, and plotted in the control space (u_x, u_y in this case). The size of the ellipse reflects the eigenvalues of the haptic metric: a larger ellipse corresponds to smaller eigenvalues. Near the boundary of the staircase, the ellipses are larger, indicating that manipulating the pendulum is easier at its tip than at its origin. Additionally, the orientation of the ellipse provides insights. The long axis, representing the direction of lower eigenvalue, shows that it is easier to push the pendulum along the tangent direction at the tip. Conversely, squeezing the pendulum results in a larger eigenvalue, represented by the short axis of the ellipse.

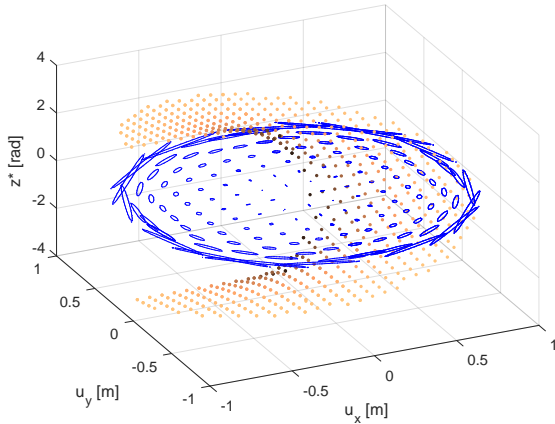


Fig. 2: Haptic metric in control space \mathcal{U} in the example of inverted pendulum.

Following [17], for control policy $\mathbf{u} : [0, 1] \rightarrow \mathbb{R}^K$ connecting two points in the control space, haptic distance S between any two points $\mathbf{u}(0)$ to $\mathbf{u}(1)$ is defined as,

$$S[\mathbf{u}] = \int_0^1 \sqrt{\dot{\mathbf{u}}^T \mathbf{G}_m^2(\mathbf{z}^*(\mathbf{u}), \mathbf{u}) \dot{\mathbf{u}}} dt \quad (4)$$

The greater the force required by robot during manipulation, the larger the value of S . However, since $\mathbf{G}_m(\mathbf{z}^*(\mathbf{u}), \mathbf{u})$ depends on $\mathbf{z}^*(\mathbf{u})$, and the equilibrium manifold is defined implicitly, the value of $\mathbf{z}^*(\mathbf{u})$ remains unknown. The next step, therefore, is to determine a method for computing $\mathbf{z}^*(\mathbf{u})$.

C. Exploring implicit manifold via adaptive ODE

To compute $\mathbf{z}^*(\mathbf{u})$ online, we propose an adaptive algorithm to explore the implicit manifold. This method initiates from a point $(\mathbf{z}_0^*, \mathbf{u}_0)$ to updates the state \mathbf{z} in the equilibrium manifold as the control \mathbf{u} moves along the direction $\dot{\mathbf{u}}$. A first order approximation on the equilibrium manifold is given as,

$$\dot{\mathbf{z}} = -(\partial_{\mathbf{z}\mathbf{z}}^2 W)^{-1} \partial_{\mathbf{u}\mathbf{z}}^2 W \dot{\mathbf{u}} \quad (5)$$

¹In fact, as shown in [17] the matrix \mathbf{G} is a map between the tangent spaces of the control \mathbf{u} and the control force \mathbf{f}_{ctrl} . Since \mathbf{G} is symmetric, $\mathbf{M}_u = \mathbf{G}^T \mathbf{G}$ is actually the pullback metric on the control.

Eq. 5 is depicted as blue arrow in Fig. 3, illustrating the linear relationship between the infinitesimal changes in \mathbf{z} and \mathbf{u} . Computing an implicit manifold from a given set of (nonlinear) equations typically relies on standard iterative methods, such as the Newton-Raphson method, as seen in [6]. [23] has shown that the classical Newton-Raphson method can be reformulated as an adaptive ODE. Based on quasi-static assumptions, we propose tracking the evolution $t \rightarrow \mathbf{z}(t) \in \mathbb{R}^N$ as the control parameters $t \rightarrow \mathbf{u}(t) \in \mathbb{R}^K$ by numerically solving a set of adaptive ODE. The Newton-Raphson 'infinitesimal' adjustments (Eq. 6), when \mathbf{u} is held constant, lead to out-of-equilibrium dynamics, represented by the red arrow in Fig. 3.

$$\dot{\mathbf{z}} = -\eta(\partial_{\mathbf{z}\mathbf{z}}^2 W)^{-1} \partial_{\mathbf{z}} W, \quad (6)$$

where η represents step size in the ODE [23], which influences the convergence of the ODE. If η is too small, the ODE may fail to converge within the given time. Conversely, if η is too large, the ODE might jump to a different branch of the \mathcal{M}^{eq} . Combining both the behaviors (Eq. 6) and (Eq. 5) we can define the compound dynamics as $\dot{\mathbf{z}}$,

$$\dot{\mathbf{z}} = -(\partial_{\mathbf{z}\mathbf{z}}^2 W)^{-1} \partial_{\mathbf{u}\mathbf{z}}^2 W \dot{\mathbf{u}} - \eta(\partial_{\mathbf{z}\mathbf{z}}^2 W)^{-1} \partial_{\mathbf{z}} W \quad (7)$$

which is represented as the dot-line curve on \mathcal{M}^{eq} in Fig. 3. To sum up, this method allows to lift a curve $\mathbf{u}(t)$ on the control space onto the equilibrium manifold, plotted as dot-line curve.

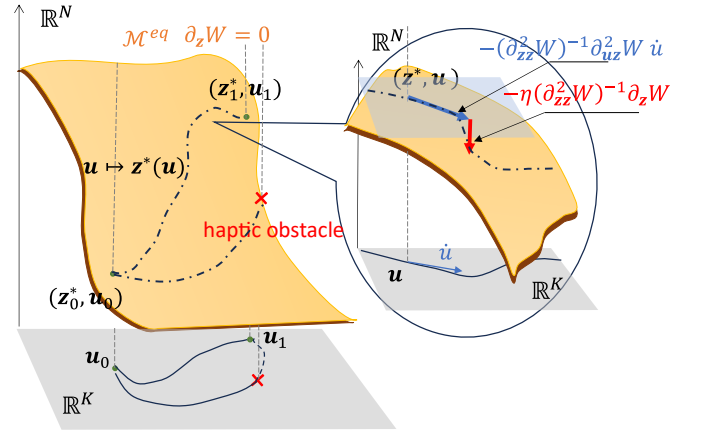


Fig. 3: Adaptive ODE allows to lift control policy $\mathbf{u}(t)$ onto \mathcal{M}^{eq} . \mathbf{u} is extended by moving along $\dot{\mathbf{u}}$ and updating \mathbf{z} on the \mathcal{M}^{eq} via Eq. 7. Blue arrow denotes \mathbf{z} linear approximation as the variation of \mathbf{u} , red arrow represents Newton-Raphson 'infinitesimal' adjustment. Some policy can be terminated by haptic obstacle.

D. Haptic Obstacle

In manipulation tasks, certain obstacles cannot be traversed by the robot. Within our configuration space, we require the node must always remain on the \mathcal{M}^{eq} . Therefore, we define a haptic obstacle as follows:

$$\det(\partial_{\mathbf{z}\mathbf{z}}^2 W(\mathbf{z}^*(\mathbf{u}), \mathbf{u})) \geq \lambda > 0 \quad (8)$$

Eq. 8 consists of two components. The term $\lambda > 0$ indicates the Hessian is positive definite, suggesting the node is stable on the equilibrium manifold [17]. The condition $\det(\partial_{\mathbf{z}\mathbf{z}}W(\mathbf{z}, \mathbf{u})) \geq \lambda$ is imposed because the inverse of Hessian is required in Eq. 7. $(\partial_{\mathbf{z}\mathbf{z}}^2 W)^{-1}$ should be sufficiently small to avoid \mathbf{z} change significantly. Otherwise, the node may inadvertently jump from one branch of the equilibrium manifold to another, as shown in Fig. 3.

III. CROWDED BOOKSHELF INSERTION

In this section, we introduce our bookshelf model, which incorporates the superellipse representation, proxies, and an augmented ODE. Traditional motion planners struggle in this context due to the limited space available for inserting a new book. In contrast, our haptic framework effectively handles uncontrollable objects, captures contact interactions, and employs a haptic metric to evaluate the optimality of the insertion process. This method enables us to tackle the challenges inherent in the crowded bookshelf insertion task.

A. Superellipses and proxy

To ensure system differentiability and support the definition of a potential function, since most simulators do not inherently provide such information, we use superellipses to represent the geometry of the books and introduce proxies to capture the contact points.

1) *Superellipses*: Since books are typically rectangular, we use superellipses (SQ) to represent them. A SQ is implicitly defined by the equation:

$$\left(\frac{x}{a_1}\right)^{\frac{2}{\epsilon}} + \left(\frac{y}{a_2}\right)^{\frac{2}{\epsilon}} = 1 \quad (9)$$

Here, ϵ controls the shape of the SQ, while a_1 and a_2 define its size. Additionally, define an inside-outside function $F(x, y)$ as

$$F(x, y) = \left(\frac{x}{a_1}\right)^{\frac{2}{\epsilon}} + \left(\frac{y}{a_2}\right)^{\frac{2}{\epsilon}} - 1 \quad (10)$$

The function $F(x, y)$ possesses a useful property. For a point (x_0, y_0) , if $F(x_0, y_0) > 0$, the point is outside the SQ. If $F(x_0, y_0) = 0$, the point lies on the surface, and if $F(x_0, y_0) < 0$, the point is inside. Due to this property, the function F is also referred to as the **inside-outside** function. Analogous to a circle, a SQ can be parameterized by angular parameterization γ as follows [24],

$$\begin{aligned} \mathbf{p}(\gamma) &= \mathbf{r}(\gamma) \begin{bmatrix} \cos \gamma \\ \sin \gamma \end{bmatrix}, 0 \leq \gamma \leq 2\pi \\ \mathbf{r}(\gamma) &= \frac{1}{\sqrt{\left(\frac{\cos \gamma}{a_1}\right)^{\frac{2}{\epsilon}} + \left(\frac{\sin \gamma}{a_2}\right)^{\frac{2}{\epsilon}}}}. \end{aligned} \quad (11)$$

2) *Proxy*: We utilize variable γ to represent the contact point $\mathbf{p}(\gamma) \in \mathbb{R}^2$ on the book, referred to as *proxy*. This allows us to represent contact interactions using both the proxy and the inside-outside function. Define a book $\mathbf{z}_b = [z_x, z_y, z_\theta]^T \in SE(2)$, symbolize one corner of a book \mathbf{z}_b as $\mathbf{c}(\mathbf{z})$ with a

corresponding proxy on another book. The proxy represents the contact point, so it should be the closest point to the corner. This condition can be expressed as:

$$\arg \min_{\gamma} : \|\mathbf{c}(\mathbf{z}) - \mathbf{p}(\gamma)\|, \gamma \in [0, 2\pi] \quad (12)$$

Meanwhile, the nonlinear stiffness k between contact points can be modeled using the signed distance $d = F(\mathbf{c})$ in book frame.

$$k(d) = k_{\min} + \frac{1 - \tanh(d/d_0)}{2} k_{\max}. \quad (13)$$

Here, d regularizes mechanical contact. If $d < 0$, it indicates contact between the two books, leading to a large contact force due to the high stiffness k_{\max} . Conversely, when there is no contact ($d > 0$), the contact force should be negligible, reflected by a significantly lower stiffness ($k_{\max} \gg k_{\min}$). The idea of proxy and SQ are illustrated in Fig. 4.

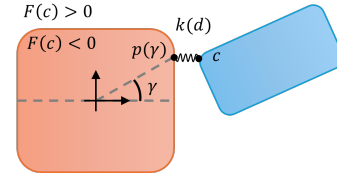


Fig. 4: Proxy on superellipse.

B. Crowded bookshelf model

As depicted in Fig. 5, a robot manipulates a book within a 2D space, defined by $\mathbf{u} = [u_x, u_y, u_\theta]^T \in SE(2)$. The gripper, employing impedance control, grasps the book using a diagonal stiffness matrix \mathbf{K}_c . The book in the robot's gripper is described by $\mathbf{z}_b = [z_x, z_y, z_\theta]^T \in SE(2)$, while other two books on the shelf are represented by $\mathbf{z}_1, \mathbf{z}_2$, each possessing only 2 DOF allowing horizontal movement and rotating ($z_{ix}, z_{i\theta}$, $i = 1, 2$). The resistive properties of the books are modeled as springs with a constant diagonal stiffness matrix $\mathbf{K}_i = \text{diag}(k_{ix}, k_{i\theta})$. The initial position (equilibrium position) is labeled as $\mathbf{z}_{i,0}$. Moreover, the contact between books is captured by proxy. We denote corner as \mathbf{c}_{ij} , and the position of proxy as $\mathbf{p}_{ij}(\gamma_j)$, where i denotes the index of object and j denotes the index of corner. For each corner j , there is a corresponding proxy parameterized by γ_j . The number of proxies N_p equals the number of corners. Symbolize as all proxy variable as $\mathbf{\Gamma} \in \mathbb{T}^{N_p}$.

Ultimately, we consider four proxy pairs ($N_p = 4$): one corner on book \mathbf{z}_1 , one corner on book \mathbf{z}_2 , two corners on book \mathbf{z}_b . Consequently, the configuration is defined by, $\mathbf{z} = [\mathbf{z}_b, \mathbf{z}_1, \mathbf{z}_2, \mathbf{\Gamma}]^T$. The manipulation potential equals,

$$\begin{aligned} W(\mathbf{z}^*, \mathbf{u}) &= W_{\text{ctrl}} + W_{\text{resist}} + W_{\text{contact}}, \\ &= \frac{1}{2}(\mathbf{u} - \mathbf{z}_b)^T \mathbf{K}_c (\mathbf{u} - \mathbf{z}_b) \\ &+ \sum_{i=1,2} \frac{1}{2}(\mathbf{z}_i - \mathbf{z}_{i,0})^T \mathbf{K}_i (\mathbf{z}_i - \mathbf{z}_{i,0}) \\ &+ \sum_i \sum_j \frac{1}{2} k(d_{ij}) \|\mathbf{c}_{ij}(\mathbf{z}_i) - \mathbf{p}_{ij}(\gamma_j)\|^2 \end{aligned} \quad (14)$$

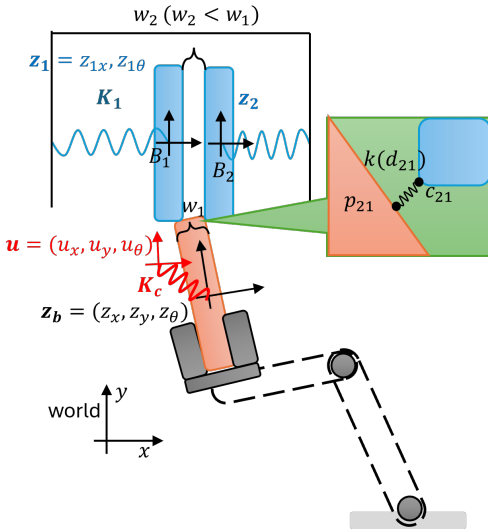


Fig. 5: A book need to be inserted to a narrow shelf, where the remaining space is not enough for insertion. The manipulated book \mathbf{z}_b is controlled with impedance control policy \mathbf{u} . Contact interaction is captured by proxy, and the resistance among the books on the bookshelf is captured by resistive spring \mathbf{K}_i .

This potential consists of three parts: W_{ctrl} denotes control energy, W_{resist} accounts for the stiffness of the other books on the shelf. W_{contact} captures the contact interaction between the manipulated book and the neighboring books. Other derivative terms and the haptic metric can be easily derived from the potential analytically.

C. Augmented adaptive ODE

We utilize Dynamic Motion Primitives (DMP) [25] to represent our control $\mathbf{u}(t)$, where K -dimensional controls (or *policies*) $t \mapsto \mathbf{u}_{\Theta}(t) \in \mathbb{R}^K$. DMP can also be viewed as a set of ODE, designed as nonlinear attractor systems that solve for a path from initial conditions to a final state. Classical DMP can be used to map a finite dimensional set of parameters $\Theta \in \mathbb{R}^{K \times P}$ where P is the number of Radial Basis Functions (RBFs) per degree-of-freedom (DOF) into smooth and differentiable functions.

$$\text{DMP} : (\Theta, \mathbf{u}_0, \mathbf{u}_T, T) \mapsto (\mathbf{u}_{\Theta}(t)) \quad (15)$$

while satisfying the boundary conditions $\mathbf{u}_{\Theta}(0) = \mathbf{u}_0$ and $\mathbf{u}_{\Theta}(T) = \mathbf{u}_T$, where T represents the duration of the intended control input. The initial condition of the robot \mathbf{u}_0 is known from the robot state, while the final state \mathbf{u}_T is the empty space between neighboring books. Thus, we combine all the

ODEs as follows,

$$\tau \dot{\mathbf{u}} = \mathbf{v}, \quad (16a)$$

$$\tau \dot{\mathbf{v}} = \alpha_v (\beta_v (\mathbf{u}_T - \mathbf{u}) - \mathbf{v}) + \mathbf{f}(\mathbf{x}), \quad (16b)$$

$$\dot{\mathbf{z}} = \begin{bmatrix} \mathbb{I}^{N-N_p} & \mathbf{0} \\ \mathbf{0} & \mathbb{I}^{N_p} \end{bmatrix} (-\partial_{\mathbf{z}\mathbf{z}}^2 W)^{-1} \partial_{\mathbf{u}\mathbf{z}}^2 W \mathbf{v} - \eta (\partial_{\mathbf{z}\mathbf{z}}^2 W)^{-1} \partial_{\mathbf{z}} W - \alpha_p \partial_{\mathbf{z}} W, \quad (16c)$$

$$\dot{\phi} = \sqrt{\mathbf{v}^T \mathbf{G}_m^2(\mathbf{u}) \mathbf{v}} \quad (16d)$$

Eq.16a and Eq.16b are same equations in DMP, denoting the attractor system. Eq. 16c comes from adaptive ODE (Eq.7) and Eq.12, the first mask matrix separate objects and proxies, \mathbb{I}^{N-N_p} multiply with adaptive ODE. The term with \mathbb{I}^{N_p} (so the last term in bracket) computes the velocity of proxies, transferring a minimization problem (Eq.12) into an ODE. The (fastest) proxy dynamics are determined by the proxy damping constant α_p . The cost function ϕ (Eq.16d) quantifies the effort required when the robot follows a control policy \mathbf{u} . The greater the force required by the robot during manipulation, the larger the value of ϕ . Meanwhile, we also setup geometric constraints for \mathbf{z} , ensuring the exploration remains within the workspace.

D. Black-Box Optimization

Following our previous work [26], as illustrated in the grey block in Fig.6. Given any initial position \mathbf{u}_0 , target \mathbf{u}_T and time duration T , we use BBO to find the optimal parameter $\hat{\Theta}$ for DMPs. In each iteration, we sample the parameter $\Theta_r \sim \mathcal{N}(\hat{\Theta}, \Sigma_{\Theta})$ based on optimal parameter in last iteration. After feeding these parameters into our augmented ODE (Eq. 16), we compute corresponding \mathbf{z}_r and its cost ϕ_r . Subsequently, the optimal parameter is updated.

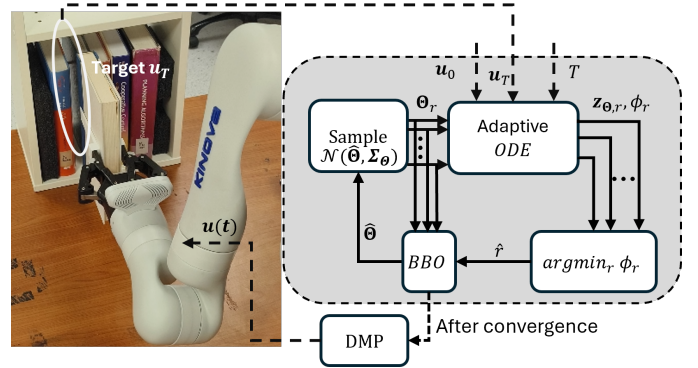


Fig. 6: our BBO framework performs multiple rollouts with different DMP parameters, Θ^r , calculating the corresponding cost (haptic distance) ϕ^r for each rollout. The optimal parameter, $\hat{\Theta}$, is then updated, and this process is repeated until the cost converges.

After the cost converges, the optimal parameters are used to generate a control trajectory via DMP, specifically utilizing the first two rows in our augmented ODE (Eq. 16). This control policy, $\mathbf{u}(t)$, is then sent to the robot for real world implementation.

IV. EXPERIMENT VALIDATION

Fig. 7a illustrates our experimental setup. We use a Kinova to manipulate a book, with two long fingers grasping the book. The Kinova is controlled in 2D. The books are manually placed on the bookshelf, where the remaining gap w_2 is narrower than the manipulated book's width w_1 . Two pieces of foam are used to adjust the stiffness of the setup.



(a) Experiment setup: The remaining space w_2 on the shelf is less than the width of the manipulated book w_1 .

(b) Stiffness calibration: Manually put the book onto the crowded shelf, then control the robot with a constant force or torque.

Fig. 7: Experiment setup and stiffness calibration.

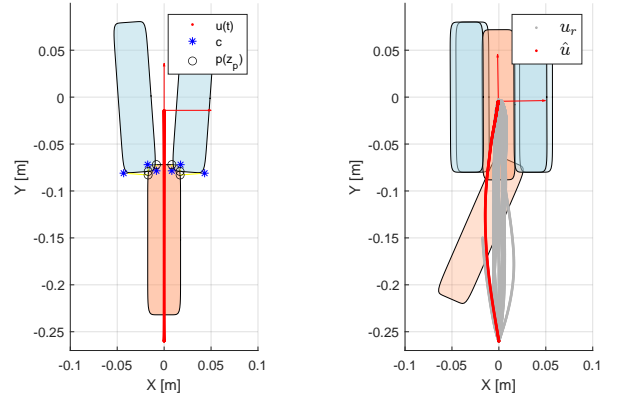
A. Experiment: Stiffness calibration

To accurately simulate the interaction with the books on the shelf, we first conduct a pre-calibration to determine their stiffness. As illustrated in Fig. 7b, we place the book in the slot and apply a constant force of 20 N or a torque of 5 Nm to the robot. The resulting displacement or rotation of the book along the z-axis is recorded. From this, we determine the stiffness to be $k_{ix} = 350 \text{ N/m}$, $k_{i\theta} = 20 \text{ Nm/rad}$.

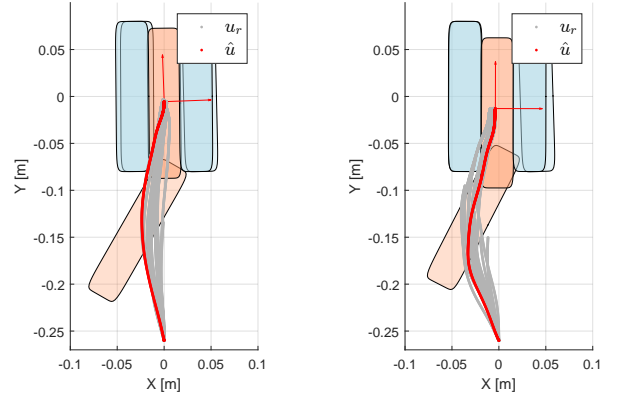
B. Simulation: Policy improvement during BBO

In this section, we demonstrate how the policy is improved based on our cost function ϕ . We select a control stiffness $k_{cx} = k_{cy} = 800 \text{ N/m}$, $k_{c\theta} = 20 \text{ Nm/rad}$. Each iteration consists of $R = 15$ rollouts. The parameter of DMP is initialized as $\Theta = \mathbf{0}$, which corresponds to a straight-line trajectory, as shown in Fig. 8a. A straight insertion policy fails due to the crowded shelf. Meanwhile, the corner of book \mathbf{c} and proxy on another book \mathbf{p} are plotted, with a yellow line connecting these proxy-corner pairs. We observe overlap between the manipulated book and the neighboring book (blue), where the corner of the manipulated book penetrates into the neighboring book. This penetration results in a high stiffness due to the non-linear stiffness model (Eq. 13), causing the book to become stuck.

The three subfigures in Fig. 8 illustrate the policy improvement across iterations. The optimal policy, $\hat{\mathbf{u}}(t)$, is selected



(a) Initial condition, straight inser-tion results failure (b) Iteration 1: $\phi = 27.96$, push with front



(c) Iteration 3: $\phi = 23.65$, push with side (d) Iteration 10: $\phi = 22.06$, push with side

Fig. 8: all variations in iteration.

based on the cost function ϕ , while non-optimal policies are shown in grey. We display the entire trajectory, $\mathbf{u}(t)$, along with two states of the books: the initial contact and the final state. Remarkably, after just one iteration (15 explorations), the robot manages to insert the book with a tilt angle. However, this policy results in a large contact force. According to our methodology, the control force can be calculated as $-\partial_{\mathbf{u}}W$. In Fig. 9, we plot the three dimensions of this control force. The grey value of the trajectories corresponds to the iteration number, allowing us to observe policy improvement over iterations. Early iterations are represented with lighter color, while the final optimal policy is shown in black. Notably, the initial iterations exhibit substantial contact forces.

In Fig. 8c and Fig. 8d, we observe that at the initial contact, the book tilts more, using its long side (the front page) to push against the neighboring book on the left, rather than the short side as seen in iteration 1 in Fig. 8a. This adjustment is reasonable, as contacting with the long side reduces the moment arm on the book, thereby decreasing the required control force and torque. This trend is evident in Fig. 9, where the optimal policy (the black curve) is closest to zero. Additionally, we notice a rapid decrease in contact force over

the first few iterations, with the policy converging in later iterations. Note that some policies fail to reach the target, indicating that the ODE was terminated either due to a haptic obstacle or because \mathbf{z} moved out of the workspace.

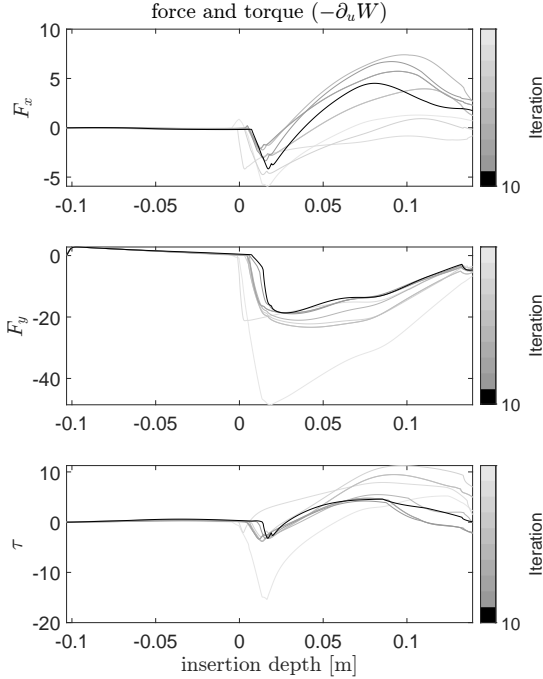


Fig. 9: Optimal control force in each iteration, iteration is shown as gray value.

C. Experiment: Qualitative results analysis

To represent control noise, we introduce similar Gaussian variations in BBO to the optimal control policy parameters, $\hat{\Theta}$. This results in similar contact forces and torques, represented by the black lines in Fig. 10. Subsequently, we utilize a Gaussian Mixture Model (GMM), shown in green, and Gaussian Mixture Regression (GMR), in pink [27] to statistically analyze the optimal policy. Due to the quasi-static assumption, we plot insertion depth [14] versus force instead of time. On the right side, we repeat the optimal policy in the real world 5 times. Because of control noise and the need to manually reposition the books on the shelf, there are minor differences in each trial. The original force data is plotted in black, with the GMM and GMR analysis following the same color scheme.

Although the insertion policy is discovered by our framework, using statistical clustering methods GMM, we can *interpret* its strategy through 5 distinct phases.

- Before contact: Both force and torque feedback are zero as the robot adjusts the book’s pose. In simulation, this is represented by a single Gaussian (the first green ellipse), while in real-world data, two Gaussians are required for the cluster. This discrepancy may arise from the joint torque sensor capturing the robot’s inertial effects.
- Push aside: The book tilts to push the neighboring book aside, requiring a torque and resistance force, hence all of them start increasing.

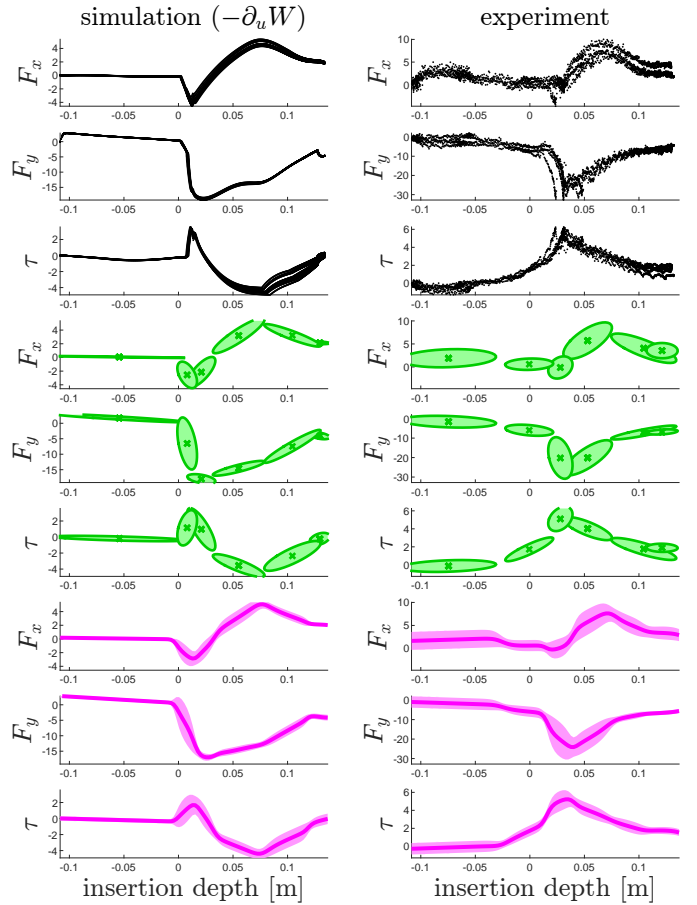


Fig. 10: Simulated contact force $-\partial_{\mathbf{u}}W$ (with exploration variation) v.s. experimental contact force, all in book frame. Black: original data. Green: cluster by GMM. Pink: regression by GMR.

- Push forward: Once the gap becomes wide enough for insertion, the robot begins pushing forward. During this phase, resistance force in y axis (push in direction) decreases, but during alignment, force in x axis is varying.
- Slide in: The robot slides the book fully into the gap, with the force and torque decreases as the book’s orientation becomes more aligned.
- Finish: All the force and torque converges in the end.

Thus, our framework autonomously discovers an explainable insertion strategy. Meanwhile, we notice the trend of contact force and torque are similar.

D. Variation of the book’s initial position

Refer to Fig. 6, we uniformly vary the initial position of the book and apply the same BBO framework to evaluate the robustness of our algorithm. Each optimal control trajectory, $\mathbf{u}(t)$, is then implemented in the real world and tested five times per case. The results, summarized in Table I, show that all cases were successful, demonstrating the effectiveness and reliability of our framework.

TABLE I: Variation of book’s initial position.

Initial position in x axis (m)	0	0.025	0.050	0.075	0.100
Successful Result	5/5	5/5	5/5	5/5	5/5

E. Variation of resistive stiffness on the shelf

In this test, we significantly increased the resistive stiffness on one side of the neighboring book. This setup represents the left side as the edge of the bookshelf, while the right side consists of regular books. Our framework discovers a different insertion policy, as shown in Fig.11. One key observation is that the manipulated book does not push against the left side (bookshelf edge), as the large stiffness results in a high value for $G(z^*(\mathbf{u}), \mathbf{u})$, leading to a high cost. This policy can be *interpreted* by 3 phases. In the left subfigure, the book

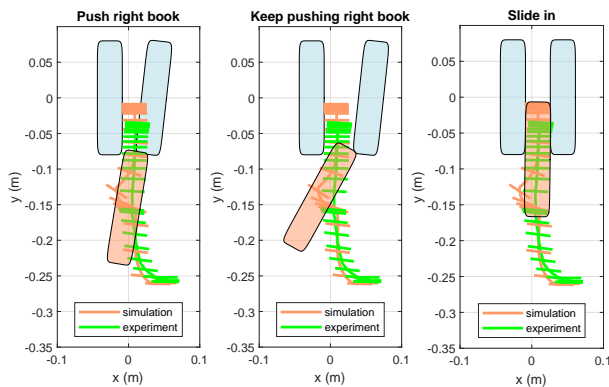


Fig. 11: Representative states when the left side is rigid. Our framework identifies the need to apply greater force on the right side (common books) until a sufficient gap is created.

pushes against the right-side book to adjust its orientation. In the middle subfigure, the robot continues pushing to create sufficient space. Finally, in the right subfigure, the book slides smoothly into the gap without pressing on the left side. This strategy proves effective in the real world, even though the book temporarily sticks at the shelf front (seen by the accumulated dash line around $y = -0.15$). However, a difference emerges during the second phase: while our SQ model results in a tilt angle of the manipulated book due to its rigid, quasi-static assumptions, real-world interactions show deformation and slip at the spine of the right adjacent book as the robot keeps pushing. Despite this discrepancy, our strategy successfully inserts the book into the shelf.

We set up 2 scenarios for this test: with the left side as the bookshelf edge and the right side as the edge. Each scenario is tested 5 times, and the results are summarized in Table II. The outcomes demonstrate that our method successfully identifies effective strategies based on the specific edge conditions.

V. CONCLUSION

In this work, we present a haptic manipulation planning framework within a naturally separated configuration space. We apply an augmented algorithm to explore the implicit

TABLE II: Variation of resistive stiffness.

Edge of bookshelf	Left Edge	Right Edge
Successful Result	5/5	5/5
Discovered strategy	Push right book	Push left book

defined manifold, computing the contact point (proxy) and haptic distance via a haptic metric. Our framework is verified on a novel task: crowded book insertion. Note we do not need any special cost design but only a manipulation potential. With the use of BBO, our framework discovers different strategic insertion policies under varying stiffness conditions and initial positions conditions. We also observe the contact force and torque decreases during optimization. These control policies are tested in the real world. The results demonstrate that, without a wedging-in strategy, direct insertion fails, highlighting the necessity of the discovered strategic insertion. Furthermore, our SQ and proxy models accurately capture most contact interactions, closely matching real-world scenarios, except for deformation and slip effects.

However, we use the spine side of the book for insertion, as inserting with the page side could lead to failure. This is due to the book cover extending beyond the pages, which increases the risk of the cover getting stuck during rotation. Additionally, we rely solely on the Kinova joint sensor without compensating for inertia, which results in non-zero values during the non-contact phase. In the future, we plan to conduct a more detailed quantitative analysis of forces with improved sensor calibration. Additionally, we will strive to prove the optimality of our policies numerically in real-world experiments.

REFERENCES

- [1] M. Suomalainen, Y. Karayiannidis, and V. Kyriki, “A survey of robot manipulation in contact,” *Robotics and Autonomous Systems*, vol. 156, p. 104224, 2022.
- [2] Z. Kingston, M. Moll, and L. E. Kavraki, “Sampling-based methods for motion planning with constraints,” *Annual review of control, robotics, and autonomous systems*, vol. 1, pp. 159–185, 2018.
- [3] M. Bonilla, L. Pallottino, and A. Bicchi, “Noninteracting constrained motion planning and control for robot manipulators,” in *2017 IEEE International Conference on Robotics and Automation (ICRA)*, pp. 4038–4043, IEEE, 2017.
- [4] J. E. Dennis Jr and R. B. Schnabel, *Numerical methods for unconstrained optimization and nonlinear equations*. SIAM, 1996.
- [5] B. Kim, T. T. Um, C. Suh, and F. C. Park, “Tangent bundle RRT: A randomized algorithm for constrained motion planning,” *Robotica*, vol. 34, no. 1, pp. 202–225, 2016.
- [6] L. Jaillet and J. M. Porta, “Path planning under kinematic constraints by rapidly exploring manifolds,” *IEEE Transactions on Robotics*, vol. 29, no. 1, pp. 105–117, 2012.
- [7] Z. Kingston, M. Moll, and L. E. Kavraki, “Exploring implicit spaces for constrained sampling-based planning,” *The International Journal of Robotics Research*, vol. 38, no. 10-11, pp. 1151–1178, 2019.
- [8] A. S. Morgan, K. Hang, B. Wen, K. Bekris, and A. M. Dollar, “Complex in-hand manipulation via compliance-enabled finger gaing and multi-modal planning,” *IEEE Robotics and Automation Letters*, vol. 7, no. 2, pp. 4821–4828, 2022.
- [9] S. Wu, J. Zhang, and D. Wu, “Equilibrium manipulation planning for a soft elastic rod considering an external distributed force and intrinsic curvature,” *IEEE Robotics and Automation Letters*, vol. 7, no. 4, pp. 11442–11449, 2022.

- [10] Í. Elguea-Aguinaco, A. Serrano-Muñoz, D. Chrysostomou, I. Inziarte-Hidalgo, S. Bøgh, and N. Arana-Arexolaleiba, "A review on reinforcement learning for contact-rich robotic manipulation tasks," *Robotics and Computer-Integrated Manufacturing*, vol. 81, p. 102517, 2023.
- [11] Y. Fan, X. Li, K. Zhang, C. Qian, F. Zhou, T. Li, and Z. Huang, "Learning robust skills for tightly coordinated arms in contact-rich tasks," *IEEE Robotics and Automation Letters*, 2024.
- [12] O. Azulay, M. Monastirsky, and A. Sintov, "Haptic-based and $se(3)$ -aware object insertion using compliant hands," *IEEE Robotics and Automation Letters*, vol. 8, no. 1, pp. 208–215, 2022.
- [13] F. Stulp and O. Sigaud, "Robot skill learning: From reinforcement learning to evolution strategies," *Paladyn, Journal of Behavioral Robotics*, vol. 4, no. 1, pp. 49–61, 2013.
- [14] D. E. Whitney *et al.*, "Quasi-static assembly of compliantly supported rigid parts," *Journal of Dynamic Systems, Measurement, and Control*, vol. 104, no. 1, pp. 65–77, 1982.
- [15] A. Salem and Y. Karayiannidis, "Robotic assembly of rounded parts with and without threads," *IEEE Robotics and Automation Letters*, vol. 5, no. 2, pp. 2467–2474, 2020.
- [16] T. Davchev, K. S. Luck, M. Burke, F. Meier, S. Schaal, and S. Ramamoorthy, "Residual learning from demonstration: Adapting dmeps for contact-rich manipulation," *IEEE Robotics and Automation Letters*, vol. 7, no. 2, pp. 4488–4495, 2022.
- [17] D. Campolo and F. Cardin, "A basic geometric framework for quasi-static mechanical manipulation," *arXiv preprint arXiv:2307.10489*, 2023.
- [18] D. Campolo and F. Cardin, "Quasi-static mechanical manipulation as an optimal process," in *2023 62nd IEEE Conference on Decision and Control (CDC)*, pp. 4753–4758, IEEE, 2023.
- [19] B. Siciliano, "Springer handbook of robotics," *Springer-Verlag google schola*, vol. 2, pp. 15–35, 2008.
- [20] A. Fischer-Cripps, "The hertzian contact surface," *Journal of materials science*, vol. 34, no. 1, pp. 129–137, 1999.
- [21] M. A. Toussaint, K. R. Allen, K. A. Smith, and J. B. Tenenbaum, "Differentiable physics and stable modes for tool-use and manipulation planning," 2018.
- [22] M. Spivak, *Calculus on manifolds: a modern approach to classical theorems of advanced calculus*. CRC press, 2018.
- [23] H. R. Schneebeli and T. P. Wihler, "The Newton–Raphson method and adaptive ODE solvers," *Fractals*, vol. 19, no. 01, pp. 87–99, 2011.
- [24] A. Jaklic, A. Leonardis, and F. Solina, *Segmentation and recovery of superquadrics*, vol. 20. Springer Science & Business Media, 2000.
- [25] A. J. Ijspeert, J. Nakanishi, H. Hoffmann, P. Pastor, and S. Schaal, "Dynamical movement primitives: learning attractor models for motor behaviors," *Neural computation*, vol. 25, no. 2, pp. 328–373, 2013.
- [26] L. Yang, M. Z. Ariffin, B. Lou, C. Lv, and D. Campolo, "A planning framework for robotic insertion tasks via hydroelastic contact model," *Machines*, vol. 11, no. 7, p. 741, 2023.
- [27] S. Kana, J. Gurnani, V. Ramanathan, M. Z. Ariffin, S. H. Turlapati, and D. Campolo, "Learning compliant box-in-box insertion through haptic-based robotic teleoperation," *Sensors*, vol. 23, no. 21, p. 8721, 2023.